Eur. Phys. J. B (2018) 91: 189
https://doi.org/10.1140/epjb/e2018-90111-0

THE EUROPEAN PHYSICAL JOURNAL B

Regular Article

On-top density in the nonlinear metallic screening and its implication on the exchange-correlation energy functional*

Yasutami Takada[a]

Institute for Solid State Physics, University of Tokyo, 5-1-5 Kashiwanoha, Kashiwa, Chiba 277-8581, Japan

Received 1 March 2018 / Received in final form 8 June 2018
Published online 29 August 2018

Abstract. In comparison with the accurate data on the on-top electron density $n(0)$ in the proton-embedded electron gas with the density parameter r_s in the range 1−12 obtained by diffusion Monte Carlo (DMC) simulations, we have successfully constructed an alternative form of the exchange-correlation energy functional in the density functional theory by imposing the constraint due to the cusp theorem on the well-known Perdew–Burke–Ernzerhof (PBE) functional. Although PBE does not, our functional, referred to as the cusp-corrected PBE (ccPBE), reproduces the DMC data on $n(0)$ in the entire range of r_s.

1 Introduction

An atom, especially hydrogen, immersed into the otherwise homogeneous electron gas (EG) has been investigated for more than four decades not only in the density functional theory (DFT), mostly in its local-density approximation (LDA) [1–14], but also in various forms of many-body theories [15–21], including diffusion Monte Carlo (DMC) [22] and variational Monte Carlo (VMC) [23] simulations. The primary motivation of those studies is to construct an appropriate theory for the nonlinear response of metallic electrons to an impurity point charge $+Ze$, but the basic physical concept with which they were concerned remains the same as that in the linear-response theory, known as Thomas–Fermi (TF) [24,25] (or Debye and Hückel [26]) screening of the impurity charge with a short screening length $\lambda_{\rm TF}$ which is about the same as $k_{\rm F}^{-1}$, where $k_{\rm F}$ is the Fermi wave number of EG.

Recently, by studying a proton (the case of $Z = 1$) embedded in EG with use of both LDA and DMC, the present author has gained a new insight into this problem [27]; the concept of Kondo screening of the spin of hydrogen with a long screening length $\lambda_{\rm K}$ ($\gg k_{\rm F}^{-1}$) [28] is found to be relevant to this system and a sharp transition from TF to Kondo screening is shown to exist with the decrease of the metallic electron density n_0 ($=k_{\rm F}^3/3\pi^2$) from the high-density limit. At the same time, the results in DMC are found to be well approximated by those in LDA in the density region characterized by Kondo screening because of the slowly-varying nature of the electron density distribution $n(\boldsymbol{r})$ around the proton due to the long $\lambda_{\rm K}$.

In the high-density region characterized by TF screening, on the other hand, a relatively large difference can be seen in $n(\boldsymbol{r})$ between DMC and LDA. In particular, an unexpected feature of $n(\boldsymbol{r})$ is found at the proton position or the on-top density $n(0)$; in DMC, $n_{\rm DMC}(0)$, is lower than that in LDA, $n_{\rm LDA}(0)$, at high densities, namely, $r_s < 1.66$ with the conventional density parameter $r_s \equiv (\alpha k_{\rm F} a_{\rm B})^{-1}$, while the opposite is the case for $r_s > 1.66$. Here we define $\alpha = (4/9\pi)^{1/3} \approx 0.5211$ and $a_{\rm B}$ is the Bohr radius. (We will use atomic units hereafter.)

According to a physical argument [29], we obtain larger $n(0)$ for stronger exchange-correlation (xc) effect, implying that as long as we believe that $n_{\rm DMC}(0)$ is sufficiently accurate, LDA is found to provide a too strong xc effect for $r_s < 1.66$ but a too weak one for $r_s > 1.66$. This interesting crossover behavior with the increase of r_s in describing the xc effect in LDA has never been known.

Because $n(\boldsymbol{r})$ varies very weakly even for $r < \lambda_{\rm TF}$ in densely packed systems such as the high-density EG for $r_s < 1.66$, it is natural to expect that a small density-gradient correction to LDA will be enough to obtain a result of $n(0)$ much better than LDA, but actually the situation becomes worse in the generalized gradient approximation (GGA) in the Perdew–Burke–Ernzerhof (PBE) version [30,31]; namely, for $r_s < 1.66$, the difference of PBE from DMC becomes larger than that of LDA. One might imagine that not PBE but the accurate gradient expansion [32] as included in PBEsol [33,34] is needed to obtain better $n(0)$, but this is not the case; no improvement on LDA is achieved even in PBEsol. Thus we come to notice that it is a nontrivial work to reproduce $n_{\rm DMC}(0)$ for the case of $r_s < 1.66$ in the framework of GGA.

* Contribution to the Topical Issue "Special issue in honor of Hardy Gross", edited by C.A. Ullrich, F.M.S. Nogueira, A. Rubio, and M.A.L. Marques.

[a] e-mail: takada@issp.u-tokyo.ac.jp

In pursuit of a key ingredient to improve on PBE in the present problem with retaining exact conditions which make PBE reliable, as listed in Table 1 in reference [35], we come across the importance of the cusp theorem [36–38] which dictates that $n(\boldsymbol{r})$ near the impurity atom behaves rigorously in such a manner as

$$n(\boldsymbol{r}) \xrightarrow[r\approx 0]{} n_{\rm cusp}(r) \equiv n(0)\exp(-2Zr), \tag{1}$$

so as to make a compromise with the singular Coulomb potential term $-Z/|\boldsymbol{r}|$. Although $n_{\rm LDA}(\boldsymbol{r})$ satisfies equation (1), $n(\boldsymbol{r})$ in PBE or PBEsol does not, indicating that the worse performance of PBE/PBEsol in determining $n(0)$ might originate from the violation of the cusp theorem.

Generally it is not believed that we can make the cusp theorem obeyed in the framework of GGA [35,39] and it is usually thought that some form of meta-GGA [40–42] is needed to satisfy it. Therefore the inclusion of the cusp theorem into a GGA-based scheme is really a challenge. In this paper we take up this challenge and set the goal of this paper in the following way; we just try to modify the spin-resolved xc energy functional $E^{\rm xc}[n_\sigma]$ in PBE by imposing the constraint due to the cusp theorem in addition to the exact conditions already obeyed by PBE and then we tune up some free parameters involved in the modified $E^{\rm xc}[n_\sigma]$ so as to reproduce $n_{\rm DMC}(0)$ in the wide range of r_s, i.e., $1 \le r_s \le 12$ where the DMC data are available.

We will leave a comprehensive test of this modified $E^{\rm xc}[n_\sigma]$ (which will be referred to as "cusp-corrected" PBE or ccPBE) for a variety of real materials for the future, but because ccPBE provides the different results of $n(0)$ from those in PBE only for $r_s < 1.66$, ccPBE and PBE will give, more or less, similar results for almost all real materials. One important exception is the solid hydrogen under very high pressures [43,44] in which $1.1 < r_s < 1.7$. Thus ccPBE may be expected to be useful only for solid hydrogen.

This paper is organized as follows: In Section 2, we introduce the system to be treated, explain the calculation methods, and account for the issues arisen from the data calculated on $n(0)$. In Section 3, we construct ccPBE and give the calculated results for $n(0)$ in ccPBE in comparison with those in DMC. Finally in Section 4, we give a summary of this paper and make several comments.

2 Atom embedded in the jellium sphere

2.1 Hamiltonian

Because Monte Carlo simulations can treat only a finite number of electrons, let us consider not bulk jellium but a jellium sphere of radius R and average density n_0 and then put a neutral atom of atomic number Z at $\boldsymbol{r}=\boldsymbol{0}$ (the center of the sphere). The number of electrons in the jellium sphere is $4\pi R^3 n_0/3 = (R/r_s)^3$, so that the total electron number N is equal to $Z+(R/r_s)^3$, satisfying global neutrality, from which we obtain $R = (N-Z)^{1/3} r_s$.

The Hamiltonian H for electrons in this system is given as

$$H = -\sum_i \frac{\boldsymbol{\nabla}_i^2}{2} + \frac{1}{2}\sum_{i\neq j}\frac{1}{|\boldsymbol{r}_i-\boldsymbol{r}_j|} + \sum_i v_{\rm ext}(\boldsymbol{r}_i), \tag{2}$$

where the external potential working on an electron $v_{\rm ext}(\boldsymbol{r})$ is composed of the potential from the nucleus and that from the positive background, written as

$$v_{\rm ext}(\boldsymbol{r}) = -\frac{Z}{r} - \frac{N-Z}{2}\frac{3R^2-r^2}{R^3}\theta(R-r) - \frac{N-Z}{r}\theta(r-R), \tag{3}$$

with $r = |\boldsymbol{r}|$ and $\theta(x)$ the Heaviside step function. In solving equation (2), we impose the fixed boundary condition to make the wave function vanish at $|\boldsymbol{r}_i| = R$. From a computational point of view, this boundary condition is indispensable to obtain rapidly and stably convergent results in the closed-shell condition.

2.2 DFT and the Kohn–Sham scheme

In DFT, the spin-resolved ground-state density $n_\sigma(\boldsymbol{r})$ for H in equation (2) is rigorously determined by the map to a noninteracting reference system which is solved by the Kohn–Sham (KS) equation, written as

$$\left[-\boldsymbol{\nabla}^2/2 + v_\sigma^{\rm KS}(\boldsymbol{r})\right]\phi_{i\sigma}(\boldsymbol{r}) = \varepsilon_{i\sigma}\phi_{i\sigma}(\boldsymbol{r}), \tag{4}$$

where $\varepsilon_{i\sigma}$ and $\phi_{i\sigma}$ are the energy level and the normalized wave function for KS orbital i and spin σ, respectively, and $v_\sigma^{\rm KS}(\boldsymbol{r})$ is the KS potential, given by

$$v_\sigma^{\rm KS}(\boldsymbol{r}) = v_{\rm ext}(\boldsymbol{r}) + \int d\boldsymbol{r}'\,\frac{n(\boldsymbol{r}')}{|\boldsymbol{r}-\boldsymbol{r}'|} + v_\sigma^{\rm xc}(\boldsymbol{r};[n_\sigma]), \tag{5}$$

where $v_\sigma^{\rm xc}(\boldsymbol{r};[n_\sigma])$ is derived from $E^{\rm xc}[n_\sigma]$ through the functional derivative as

$$v_\sigma^{\rm xc}(\boldsymbol{r};[n_\sigma]) = \delta E^{\rm xc}[n_\sigma]/\delta n_\sigma(\boldsymbol{r}). \tag{6}$$

With use of the lowest-N_σ KS orbitals, $n_\sigma(\boldsymbol{r})$ is given by

$$n_\sigma(\boldsymbol{r}) = \sum_{i=1}^{N_\sigma} |\phi_{i\sigma}(\boldsymbol{r})|^2, \tag{7}$$

and $n(\boldsymbol{r})$ is the sum of $n_\uparrow(\boldsymbol{r})$ and $n_\downarrow(\boldsymbol{r})$. The spin density $n_\sigma(\boldsymbol{r})$ and consequently N_σ with $N = \sum_\sigma N_\sigma$ should be determined by the self-consistent solution of equations (4)–(7), together with the fixed boundary condition

$$\phi_{i\sigma}(\boldsymbol{r}) = 0, \tag{8}$$

at $r = R = (N-Z)^{1/3} r_s$. This boundary condition is imposed to make a direct comparison of the results in DFT-based schemes with those in DMC.

2.3 LSDA

In order to implement the above KS scheme, we need to know some concrete form of $E^{\rm xc}[n_\sigma(\boldsymbol{r})]$. In the local-spin density approximation (LSDA), it is given by

$$E^{\rm xc}[n_\sigma(\boldsymbol{r})] = \int d\boldsymbol{r}\, n(\boldsymbol{r})\epsilon_{\rm xc}^{\rm unif}\big(r_s(\boldsymbol{r}),\zeta(\boldsymbol{r})\big), \tag{9}$$

where $n(\boldsymbol{r}) = n_\uparrow(\boldsymbol{r}) + n_\downarrow(\boldsymbol{r})$ and $\epsilon_{\rm xc}^{\rm unif}(r_s,\zeta)$ is the xc energy per electron for the homogeneous electron gas with the density parameter $r_s = (3/4\pi n)^{1/3}$ and the spin polarization $\zeta = (n_\uparrow - n_\downarrow)/n$. Usually, $\epsilon_{\rm xc}^{\rm unif}(r_s,\zeta)$ is divided into two parts; the exchange part $\epsilon_{\rm x}^{\rm unif}(r_s,\zeta)$ and the correlation part $\epsilon_{\rm c}^{\rm unif}(r_s,\zeta)$, both of which are concretely given in reference [45], but we can simply write $\epsilon_{\rm x}^{\rm unif}(r_s,\zeta)$ as

$$\epsilon_{\rm x}^{\rm unif}(r_s,\zeta) = \epsilon_{\rm x}^{\rm unif}(r_s)\frac{(1+\zeta)^{4/3}+(1-\zeta)^{4/3}}{2}, \tag{10}$$

with $\epsilon_{\rm x}^{\rm unif}(r_s) = -(3/4)(3/2\pi)^{2/3}/r_s$.

2.4 PBE

In GGA, $E^{\rm xc}[n_\sigma(\boldsymbol{r})]$ is given as a functional of not only $n_\sigma(\boldsymbol{r})$ but also its first derivative $\boldsymbol{\nabla} n_\sigma(\boldsymbol{r})$. In its PBE version, $E^{\rm xc}[n_\sigma(\boldsymbol{r})]$ is assumed to be

$$E^{\rm xc}[n_\sigma(\boldsymbol{r})] = \frac{E^{\rm x}[2n_\uparrow(\boldsymbol{r})]+E^{\rm x}[2n_\downarrow(\boldsymbol{r})]}{2} + E^{\rm c}[n_\sigma(\boldsymbol{r})], \tag{11}$$

with the exchange energy functional $E^{\rm x}[n(\boldsymbol{r})]$, written as

$$E^{\rm x}[n(\boldsymbol{r})] = \int d\boldsymbol{r}\, n(\boldsymbol{r})\epsilon_{\rm x}^{\rm unif}(r_s)F_{\rm x}(s), \tag{12}$$

where $s = s(\boldsymbol{r})$ is the normalized derivative, defined by

$$s(\boldsymbol{r}) = \frac{|\boldsymbol{\nabla} n(\boldsymbol{r})|}{2k_F(\boldsymbol{r})n(\boldsymbol{r})} = \frac{|\boldsymbol{\nabla} n(\boldsymbol{r})|}{2(3\pi^2)^{1/3}n(\boldsymbol{r})^{4/3}}, \tag{13}$$

with $k_F(\boldsymbol{r}) = [3\pi^2 n(\boldsymbol{r})]^{1/3}$ and $F_{\rm x}(s)$ is given by

$$F_{\rm x}(s) = 1 + \kappa - \frac{\kappa}{1+\mu_{\rm PBE}s^2/\kappa}, \tag{14}$$

with $\kappa = 0.804$ and $\mu_{\rm PBE} = 0.21951$. By using $E^{\rm x}[n(\boldsymbol{r})]$ in equation (12), we can derive $v_\sigma^{\rm x}(\boldsymbol{r})$ the exchange part of $v_\sigma^{\rm xc}(\boldsymbol{r};[n_\sigma])$ for a spin-σ electron as

$$\begin{aligned} v_\sigma^{\rm x}(\boldsymbol{r}) &= \left.\frac{\delta E^{\rm x}[n(\boldsymbol{r})]}{\delta n(\boldsymbol{r})}\right|_{n(\boldsymbol{r})=2n_\sigma(\boldsymbol{r})} \\ &= \epsilon_{\rm x}^{\rm unif}(r_s)\left[\frac{4}{3}F_{\rm x}(s) - v\frac{\partial F_{\rm x}(s)}{s\partial s}\right. \\ &\quad \left. - \left(u - \frac{4}{3}s^3\right)\frac{\partial}{\partial s}\left(\frac{\partial F_{\rm x}(s)}{s\partial s}\right)\right], \end{aligned} \tag{15}$$

where $u = u(\boldsymbol{r})$ and $v = v(\boldsymbol{r})$ are defined, respectively, as

$$u(\boldsymbol{r}) = \frac{\boldsymbol{\nabla} n(\boldsymbol{r})\cdot\boldsymbol{\nabla}|\boldsymbol{\nabla} n(\boldsymbol{r})|}{[2k_F(\boldsymbol{r})]^3 n(\boldsymbol{r})^2},\ v(\boldsymbol{r}) = \frac{\boldsymbol{\nabla}^2 n(\boldsymbol{r})}{[2k_F(\boldsymbol{r})]^2 n(\boldsymbol{r})}. \tag{16}$$

On the other hand, the correlation energy functional $E^{\rm c}[n_\sigma(\boldsymbol{r})]$ in equation (11) is given by

$$E_c[n(\boldsymbol{r})] = \int d\boldsymbol{r}\left[\epsilon_c^{\rm unif}(r_s,\zeta) + H(r_s,\zeta,t)\right], \tag{17}$$

where the functional $H(r_s,\zeta,t)$ is defined as

$$H(r_s,\zeta,t) = \gamma\phi^3 \ln\left\{1 + \frac{\beta_{\rm MB}}{\gamma}t^2\left[\frac{1+At^2}{1+At^2+A^2t^4}\right]\right\}, \tag{18}$$

with introducing $t = (3\pi^2/16)^{1/3}s/\sqrt{r_s}\phi(\zeta)$ and the function $\phi(\zeta)$ defined as $\phi(\zeta) = [(1+\zeta)^{1/3}+(1-\zeta)^{1/3}]/2$. Here $\beta_{\rm MB} = 0.066725$ [46] and the functional A is given as

$$A = \frac{\beta_{\rm MB}}{\gamma}\left\{\exp[-\epsilon_c^{\rm unif}(r_s,\zeta)/\gamma\phi^3] - 1\right\}^{-1}, \tag{19}$$

with $\gamma = (1-\ln 2)/\pi^2$. By the functional derivative of $E^{\rm c}[n_\sigma(\boldsymbol{r})]$ with respect to $n_\sigma(\boldsymbol{r})$, we obtain $v_\sigma^{\rm c}(\boldsymbol{r})$. The concrete form for $v_\sigma^{\rm c}(\boldsymbol{r})$ is suppressed here.

In PBEsol, the same forms for the exchange and correlation energy functionals are adopted with the replacement of $\mu_{\rm PBE}$ and $\beta_{\rm MB}$ by $\mu_{\rm GE}$ (=10/81) [32] and 0.046, respectively.

2.5 DMC

The detailed account of the procedure for DMC is given in reference [27] and thus we will not recapitulate it here, but the point is that the only approximation involved in DMC is the so-called "fixed-node approximation". As explained in reference [27], we consider that unphysical node-position dependent effects will be removed by extracting the N-independent results, because the node positions depend on N in the fixed boundary condition.

As for the on-top density $n(0)$, the N-independent results are found to be obtained, if N becomes as large as about 60 for the proton-embedded EG. Furthermore, the center of the sphere is very much separated from any postulated node positions, implying that $n(0)$ is the physical quantity least affected by the fixed-node approximation. For those reasons, it is well expected that DMC provides accurate, if not exact, results for $n(0)$.

2.6 On-top density in LDA, PBE, and DMC

We have applied DMC to the system described by H in equation (2) with $Z = 1$ and, as reported in reference [27], we have obtained convergent results at $N = 58$ for $r_s \le 2.6$ (the TF-screening region) and $N = 60$ otherwise (the Kondo-screening region). In the stably convergent closed-shell condition, the doubly-degenerate $3s$ energy level corresponding to the Kondo singlet state is situated just above (below) the Fermi level for low- (high-)r_s systems,

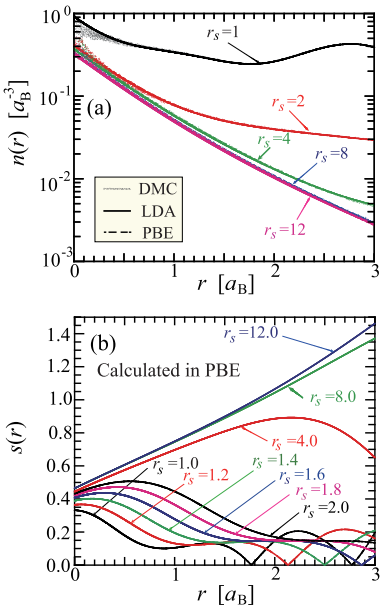

Fig. 1. (a) Density distribution $n(\boldsymbol{r})$ calculated in LDA, PBE, and DMC for the proton-embedded electron-gas sphere with the total electron number $N = 58$ for $r_s = 1$ and 2, and $N = 60$ otherwise. (b) The corresponding normalized derivative function $s(\boldsymbol{r})$ in PBE.

leading to the difference in N by 2 between the case of $r_s \leq 2.6$ and that of $r_s > 2.6$. In order to make a direct comparison with those DMC results, both LSDA and PBE have been performed in exactly the same situation as for N and the boundary condition at each r_s. Note that there is no difference between LSDA and LDA in the present system, because the ground states are always found to be paramagnetic. Thus we will simply write "LDA" hereafter, even though the actual calculations are done in LSDA.

The obtained results of $n(\boldsymbol{r})$ in both LDA and PBE are in good agreement with those in DMC, especially for r larger than $2a_B$, as seen, for example, in Figure 5 in reference [27], irrespective of either TF or Kondo region. Relatively speaking, for r less than about a_B, however, there are rather large differences among DMC, LDA, and PBE, as shown explicitly in Figure 1a and the largest deviation occurs at $r = 0$. Thus it is important to make a detailed quantitative comparison of the on-top density $n(0)$ among those calculation methods in order to assess the performance of DFT-based schemes in reference to DMC.

In view of equation (1), $n(\boldsymbol{r})$ changes linearly with the increase of r in semi-log plot, as long as r is less than about $0.3a_B$. (In dense systems like r_s less than about 2, this critical value for the cusp theorem r_{cusp} becomes smaller; it may be safe to take $0.1a_B$ for r_{cusp} at $r_s = 1$.) This linear property in semi-log plots is very useful in estimating $n(0)$ in DMC. The results so obtained for $n(0)$ in each scheme are given in Table 1, from which we find that for r_s less than about 1.66 (Region I), $n_{DMC}(0) < n_{LDA}(0) < n_{PBE}(0)$, while for larger r_s (Region II which includes the TF-Kondo transition point), $n_{DMC}(0) > n_{PBE}(0) > n_{LDA}(0)$. Note that this interesting

Table 1. On-top density $n(0)$ in atomic units for the proton-embedded electron-gas sphere with the total electron number $N = 58$ for $r_s = 1.0{-}2.6$ and $N = 60$ otherwise.

r_s	LDA	PBE	DMC
1.0	0.91886	0.92150	0.894 ± 0.034
1.2	0.69298	0.69702	0.674 ± 0.023
1.4	0.56659	0.57217	0.556 ± 0.017
1.6	0.48990	0.49706	0.486 ± 0.019
1.8	0.44076	0.44946	0.450 ± 0.014
2.0	0.40806	0.41815	0.418 ± 0.010
2.2	0.38570	0.39698	0.402 ± 0.009
2.6	0.35902	0.37198	0.382 ± 0.008
2.7	0.45749	0.46823	0.476 ± 0.007
3.0	0.42502	0.43576	0.442 ± 0.006
4.0	0.36922	0.37950	0.388 ± 0.006
5.0	0.34656	0.35639	0.359 ± 0.005
6.0	0.33550	0.34551	0.349 ± 0.003
7.0	0.32939	0.34027	0.347 ± 0.003
8.0	0.32573	0.33796	0.345 ± 0.002
9.0	0.32339	0.33718	0.343 ± 0.002
10.0	0.32182	0.33711	0.342 ± 0.001
11.0	0.32073	0.33731	0.341 ± 0.001
12.0	0.31995	0.33759	0.339 ± 0.001

crossover point from Region I to Region II is situated in the density region in which the solid hydrogen and related materials under high pressures are involved, i.e., $1.1 < r_s < 1.7$ [43,44], making the present assessment relevant and important in studying physics of the solid hydrogen in the framework of DFT.

Incidentally, in Figure 1b, the results for the normalized derivative $s(\boldsymbol{r})$ in PBE defined in equation (13), corresponding to those of $n(\boldsymbol{r})$ in Figure 1a, are plotted, revealing the interesting fact that in Region I, $s(\boldsymbol{r})$ always stays less than 0.43, but in Region II, it becomes larger than that value. It must also be noted that in the Kondo-screening regime in Region II, the behavior of $s(\boldsymbol{r})$ is much different from that in the TF-screening regime, providing another piece of evidence for the qualitative difference between those two regimes of screening.

3 Proposal of cusp-corrected PBE

3.1 Violation of the cusp theorem in PBE

Confronted with the interesting behavior of the difference between PBE and DMC with the increase of r_s in Table 1, we have made various trials to construct a new xc energy functional in GGA so that $n(0)$ in DMC can be well reproduced in the entire range of r_s, mostly by just modifying $F_x(s)$ from the original one in PBE, as is usually the case in most other modifications of $E^{xc}[n_\sigma(\boldsymbol{r})]$ from PBE, such as WC [47–49]. Incidentally, there is no problem in Region II; LDA already provides reasonably good $n(0)$ and PBE improves much on it, but it is by no means easy to obtain $n(0)$ in similar accuracy in Region I. Thus we will focus on that region in the following.

In Region I, $s(\boldsymbol{r})$ is less than 0.43 and thus we need some new insight into $E^{xc}[n(\boldsymbol{r})]$ in this small-s range. In

pursuit of the new ingredient needed for improving on the PBE energy functional, we have paid attention to the cusp theorem; as mentioned in Section 1, the cusp behavior in equation (1) is correctly reproduced in LDA, but it is usually not the case in GGA due to the appearance of a singular term $-\delta Z/|\boldsymbol{r}|$ in the exchange-correlation potential $v^{\rm xc}(\boldsymbol{r})$ near the nucleus, in addition to the external singular term $-Z/|\boldsymbol{r}|$. In the presence of this additional singular term, the cusp behavior is not determined by Z but $Z+\delta Z$, leading to the relative error in proportion to $\delta Z/Z$.

With the use of equations (1), (13), and (16), we find that for $r \approx 0$, $s(\boldsymbol{r})$, $u(\boldsymbol{r})$, and $v(\boldsymbol{r})$ behave, respectively, as

$$s(\boldsymbol{r}) \approx s_c, \quad u(\boldsymbol{r}) \approx s_c^3, \quad v(\boldsymbol{r}) \approx s_c^2 - \frac{s_c^2}{Zr}, \tag{20}$$

with $s_c \equiv Z/[3\pi^2 n(0)]^{1/3}$. Thus for $r \approx 0$, the singular contribution to $v_\sigma^{\rm x}(\boldsymbol{r})$ in equation (15) comes only from the term in proportion to $v(\boldsymbol{r})$. More explicitly, the singular term can be written as

$$-\epsilon_{\rm x}^{\rm unif}(r_s^c)\left(-\frac{s_c^2}{Zr}\right)\frac{\partial F_{\rm x}(s_c)}{s_c \partial s_c} = -\left(\frac{3}{4\pi}\frac{\partial F_{\rm x}(s_c)}{\partial s_c}\right)\frac{1}{r}, \tag{21}$$

with $r_s^c \equiv [3/4\pi n(0)]^{1/3}$. Similarly, the singular term in $v_\sigma^{\rm c}(\boldsymbol{r})$ is written in the form of equation (21) with the replacement of $F_{\rm x}(s_c)$ by $F_{\rm c}(s_c)$, defined as

$$F_{\rm c}(s_c) = \frac{\epsilon_{\rm c}^{\rm unif}(r_s^c, 0) + H(r_s^c, 0, t_c)}{\epsilon_{\rm x}^{\rm unif}(r_s^c)} \tag{22}$$

with $t_c = (3\pi^2/16)^{1/3} s_c/\sqrt{r_s^c}$. Then δZ is given by

$$\delta Z = \frac{3}{4\pi}\frac{\partial}{\partial s}(F_{\rm x}+F_c) = \frac{3}{2\pi} s \left(\frac{\partial F_{\rm x}}{\partial s^2} + \frac{\partial F_{\rm c}}{\partial s^2}\right), \tag{23}$$

evaluated at the cusp position $r=0$ with $r_s = r_s^c$, $s = s_c$, and $\zeta = 0$.

For the case of $Z \gg 1$, $n(0)$ is well approximated by either Z^3/π in the strong-correlation limit or $2Z^3/\pi$ in the weak-correlation limit. Then we obtain s_c and r_s^c, respectively, as either $(3\pi)^{-1/3} \approx 0.473$ and $(3/4)^{1/3}Z^{-1}$ or $(6\pi)^{-1/3} \approx 0.376$ and $(3/8)^{1/3}Z^{-1}$ in each limit, implying that s_c is in the range $(0.376, 0.473)$ and $r_s^c \ll 1$. However, not only in the present atom-embedded EG but also in atoms, molecules, and solids in which the condition of $Z \gg 1$ is not always satisfied, s_c varies in the range from 0.32 to 0.473, still a relatively small range of s around 0.4.

Now, let us take $F_{\rm c}$ as $F_{\rm c}^{\rm PBE}$ the one given in PBE. Then the second component in equation (23) or the function $\partial F_{\rm c}^{\rm PBE}/\partial s_c^2$ is concretely known as a function of s_c with r_s^c set equal to $(9\pi/4)^{1/3}s_c/Z$ for each Z. In Figure 2, this function (or actually its negative, $-\partial F_{\rm c}^{\rm PBE}/\partial s_c^2$) is plotted as a function of s_c, from which we see that if s_c were zero (or at least very small), the cusp condition would be (almost) fulfilled in PBE, because $\partial F_{\rm c}^{\rm PBE}/\partial s_c^2$ (which is equal to $-\mu_{\rm PBE}$ at $s_c = 0$, irrespective of Z) is cancelled by $\partial F_{\rm x}^{\rm PBE}/\partial s_c^2 = \mu_{\rm PBE}/(1+\mu_{\rm PBE}s_c^2/\kappa)^2$. In fact, in the original PBE, $\mu_{\rm PBE}$ is so determined as to satisfy this condition at $s_c = 0$, a relation to intimately connect $F_{\rm x}^{\rm PBE}$ with $F_{\rm c}^{\rm PBE}$. In the actual cusp region in which s_c is about 0.4, however, δZ is not small enough and thus the cusp theorem is violated in PBE; the relative error $\delta Z/Z$ is about 1.8% and 1.2% for $Z = 1$ and 2, respectively, and less than 1% for $Z \geq 3$.

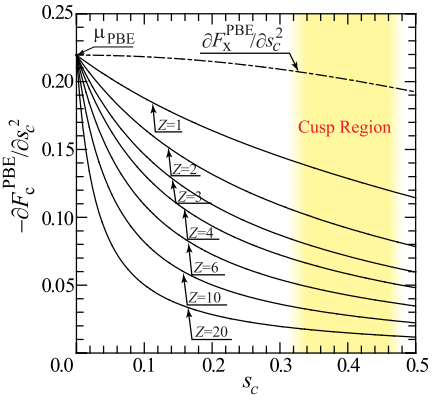

Fig. 2. "Target function" or the partial derivative of $-F_{\rm c}$ with respect to s_c^2 in PBE plotted as a function of s_c for various Z with $r_s = (9\pi/4)^{1/3}s_c/Z$. For comparison, $\partial F_{\rm x}/\partial s_c^2$ in PBE is also plotted by the dotted-dashed curve. In actual cusp positions, the value of s_c is in the range 0.32−0.473.

The above observation inspires us that if we can modify $F_{\rm x}(s)$ so as to cancel $\partial F_{\rm x}(s)/\partial s^2$ with $\partial F_{\rm c}^{\rm PBE}/\partial s^2$ for s not at a single point of $s = 0$ but in the entire cusp region of $(0.32, 0.473)$, we can always make δZ vanish at the cusp point (and thus impose the cusp theorem), whatever value for s_c is determined in the self-consistent calculation of $n(\boldsymbol{r})$. This constitutes the main idea of this paper. Of course, because $-\partial F_{\rm c}^{\rm PBE}/\partial s^2$, which will be called "the target function" hereafter, depends on Z, we have to treat its Z dependence appropriately, but for the time being, we take the target function at $Z = 1$. Then, for other values of Z the cusp theorem will be violated, but in this case the relative error $\delta Z/Z$ becomes much smaller than that in PBE; at the most, it is about 0.36% for $Z = 2$ or 3.

A formally better scheme to impose the constraint due to the cusp theorem for any Z will be mentioned in Section 4. As for the choice of $F_{\rm c}$, we have examined the case of $F_{\rm c}$ with $\beta_{\rm MB}$ in equations (18) and (19) replaced by either 0.046 as in PBEsol or the more refined r_s-dependent one, $\beta(r_s)$, expressed as [41,50]

$$\beta(r_s) = \beta_{\rm MB}\frac{1+0.1r_s}{1+0.1778r_s}, \tag{24}$$

but we find that no appreciable difference is seen in the final results for $n(0)$.

3.2 Exchange energy functional in ccPBE

In order to construct $F_{\rm x}(s)$ in accordance with the above-mentioned idea to fulfill the cusp theorem under the assumption that the correlation energy functional is set equal to $F_{\rm c}^{\rm PBE}$, we have examined a variety of possible

forms to arrive at the following $F_{\rm x}(s)$ which is given as the sum of three terms:

$$F_{\rm x}(s) = F_0(s) + F_1(s) + F_2(s), \tag{25}$$

where $F_0(s)$ is basically the one only slightly modified from the original form in PBE as

$$F_0(s) = A_0 + A_1 - \frac{A_1}{1 + \mu(p)\, p/A_1}, \tag{26}$$

where $p \equiv s^2$ and $\mu(p)$ is assumed to be

$$\mu(p) = \mu_1 + (\mu_0 - \mu_1)\exp(-p/s_0^2). \tag{27}$$

The function $F_1(s)$ is assumed to be

$$F_1(s) = B_0 \exp(-p^2/s_1^4), \tag{28}$$

in order to satisfy the exact gradient expansion (GE) of $F_{\rm x}(s)$ in the limit of $s \to 0$, known as [51]

$$F_{\rm x} = 1 + \mu_{\rm GE}\, p + \frac{146}{2015} v^2 - \frac{73}{405} p\, v + D p^2 + O(\boldsymbol{\nabla}^6), \tag{29}$$

where v is defined in equation (16) and the coefficient D vanishes according to the best numerical estimate. The function $F_2(s)$ is so introduced as to impose the constraint due to the cusp theorem; namely, $\partial F_{\rm x}(s)/\partial s^2$ is set equal to $-\partial F_{\rm c}^{\rm PBE}/\partial s^2$ with $Z = 1$ for s in the range $(0.32, 0.473)$. The actual procedure is to begin with the assumption of $F_2(s)$ in the form of

$$F_2(s) = \frac{p^2}{s_2^4}\left[C_0 + \sum_{i=1}^{6} C_i \left(\frac{p}{s_2^2}\right)^i\right]\exp(-p/s_2^2). \tag{30}$$

Then, under given values for C_0 and s_2, we determine the six coefficients, $C_1, \ldots, C_6$, so as to satisfy the above-mentioned condition for fulfilling the cusp theorem.

There are still nine parameters, s_0, s_1, s_2, A_0, A_1, μ_0, μ_1, B_0, and C_0, to be fixed, but they cannot be chosen independently; there are four important constraints; in the limit of $s \to \infty$, there is the Lieb–Oxford upper bound $1 + \kappa$ with $\kappa = 0.804$ for $F_{\rm x}(s)$ [52], leading to the condition of

$$\lim_{s\to\infty} F_{\rm x}(s) = A_0 + A_1 = 1 + \kappa. \tag{31}$$

In the limit of $s \to 0$, we should respect equation (29), but because the functional $F_{\rm x}$ in GGA is assumed to be a function of a single variable s, we need to derive an approximate expression for v in terms of s in order to make use of equation (29). As in equation (20), by the use of the definitions of s and v in equations (13) and (16), respectively, and the behavior of $n(\boldsymbol{r})$ in equation (1) near the nucleus at which the electron density varies most rapidly, we obtain

$$s = \frac{Z}{k_F} \quad \text{and} \quad v = \frac{Z^2}{k_F^2}\left(1 - \frac{1}{Zr}\right). \tag{32}$$

Table 2. Set of parameters to specify $F_{\rm x}(s)$ in ccPBE. In order to satisfy the cusp condition, three target functions corresponding to $Z = 1$, 2, and 3 are considered. Note that only the parameters $C_0, C_1, \ldots, C_6$, and s_2 depend on Z.

	$Z = 1$	$Z = 2$	$Z = 3$
A_0	1.036	1.036	1.036
A_1	0.768	0.768	0.768
μ_0	0.12345679	0.12345679	0.12345679
μ_1	0.13170898	0.13170898	0.13170898
s_0	1.20	1.20	1.20
B_0	–0.036	–0.036	–0.036
s_1	0.180	0.180	0.180
C_0	–0.006933655	–0.007332614	–0.007538429
C_1	–0.011363996	–0.036651747	–0.038238364
C_2	0.010829969	0.039997327	0.046200149
C_3	–0.003780562	–0.014587676	–0.017395384
C_4	0.000643956	0.002663050	0.003272557
C_5	–0.0000554048	–0.0002416611	–0.0003038872
C_6	0.00000197693	0.00000954069	0.00001237041
s_2	0.142	0.144	0.145

Then, v is approximately given by $v = v_0 s^2$ with a coefficient v_0 which is calculated by taking the average of $1/Zr$ by the weight of $n(0)\exp(-2Zr)$ in the range of $0 \le r \le r_{\rm cusp}$ with $r_{\rm cusp}$ which is the critical value for r satisfying the cusp condition, as introduced in Section 2.6. More specifically, v_0 is calculated as

$$\begin{aligned} v_0 &= 1 - \left\langle \frac{1}{Zr} \right\rangle = 1 - \frac{\int d\boldsymbol{r} \exp(-2Zr)/Zr}{\int d\boldsymbol{r} \exp(-2Zr)} \\ &= -\frac{\rho_0^2/2}{\exp(\rho_0) - 1 - \rho_0 - \rho_0^2/2}, \end{aligned} \tag{33}$$

with $\rho_0 = 2Zr_{\rm cusp}$. Because $r_{\rm cusp}$ is about 0.1 or larger and the case of $Z = 1$ is considered here, we take ρ_0 as 0.20 tentatively in the following. Then, we obtain the small-s expansion of $F_{\rm x}(s)$ in the following way:

$$F_{\rm x}(s) = 1 + \mu_{\rm GE}\, p + \mu_4\, p^2, \tag{34}$$

with $\mu_4 = (146/2015)v_0^2 - (73/405)v_0 \approx 17.22612$.

In accordance with the small-p expansion in equation (34), terms at each order, $O(p^0)$, $O(p)$, or $O(p^2)$, should satisfy

$$F_{\rm x}(0) = 1 = A_0 + B_0, \tag{35}$$

$$\frac{\partial F_{\rm x}(0)}{\partial p} = \mu_{\rm GE} = \mu_0, \tag{36}$$

$$\frac{1}{2}\frac{\partial^2 F_{\rm x}(0)}{\partial^2 p} = \mu_4 = \frac{\mu_1 - \mu_0}{s_0^2} - \frac{\mu_0^2}{A_1} - \frac{B_0}{s_1^4} + \frac{C_0}{s_2^4}, \tag{37}$$

respectively. By use of equations (31), (35)–(37), the parameters, A_0, A_1, μ_0, and C_0 can be determined under given values for the rest of the parameters.

By comparing the calculated results for the single-proton embedded electron-gas sphere in ccPBE with those in DMC, we can determine an appropriate set of parameters providing sufficiently good results. The

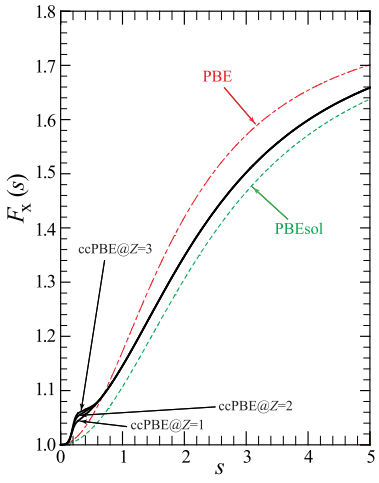

Fig. 3. $F_x(s)$ in ccPBE determined in reference to three different target functions with $Z = 1$, 2, and 3. For comparison, we also plot $F_x(s)$ in both PBE and PBEsol by dotted dashed and dotted curves.

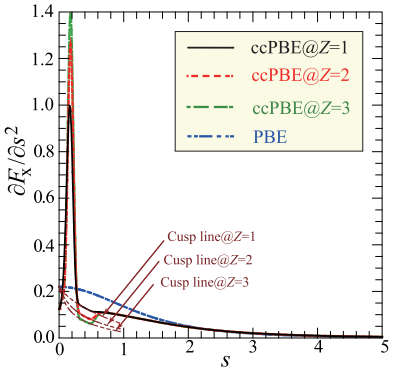

Fig. 4. $\partial F_x/\partial s^2$ corresponding to $F_x(s)$ in ccPBE in Figure 3. It coincides with the target function (or the cusp line) at each Z, plotted by the double-dotted-dashed curve, for s in the range 0.32−0.473.

parameter set so obtained is given in Table 2 in which another set of parameters fulfilling the cusp condition for $Z = 2$ and 3 are also added. Note that the parameters depending on Z are only those concerned with $F_2(s)$.

With those parameters, we can concretely give $F_x(s)$ in ccPBE and its derivative $\partial F_x(s)/\partial s^2$, both of which are plotted in Figures 3 and 4, respectively. We have plotted $F_x(s)$ for three cases of the target functions with $Z = 1$, 2, and 3, but its Z-dependence is found to be weak. Compared with $F_x(s)$ in PBE and PBEsol, $F_x(s)$ in ccPBE is enhanced much and has a characteristic structure for $s < 0.6$ but it increases smoothly for $s > 0.6$ and its actual value comes to the middle of PBE and PBEsol.

As for $\partial F_x(s)/\partial s^2$, its Z-dependence is much stronger than that for $F_x(s)$. The first sharp peak at $s \approx 0.2$ is found to be important to control the actual values of $n(0)$ for $r_s < 2$. (See the dependence of the peak structure on Z in Fig. 4 and the change of $n(0)$ with Z in Tab. 3.) This

Table 3. On-top density $n(0)$ in ccPBE for the proton-embedded electron-gas sphere with the total electron number $N = 58$ for $r_s = 1.0-2.6$ and $N = 60$ otherwise. The parameter sets are used for the target function with either $Z = 1$ or $Z = 2$. The errors are given as the relative ones in % with respect to the DMC results.

	ccPBE		ccPBE	
r_s	@$Z=1$	Error(%)	@$Z=2$	Error(%)
1.0	0.89459	0.07	0.88545	−0.96
1.2	0.67670	0.40	0.66729	−1.00
1.4	0.55895	0.53	0.54989	−1.10
1.6	0.48948	0.72	0.48177	−0.87
1.8	0.44527	−1.05	0.44013	−2.19
2.0	0.41785	−0.04	0.42272	1.13
2.2	0.40152	−0.12	0.41786	3.94
2.6	0.38202	0.01	0.40267	5.41
2.7	0.47532	−0.14	0.48558	2.01
3.0	0.44295	0.22	0.45574	3.11
4.0	0.38559	−0.62	0.40013	3.13
5.0	0.36097	0.55	0.37486	4.42
6.0	0.34917	0.05	0.36299	4.01
7.0	0.34335	−1.05	0.35682	2.83
8.0	0.34100	−1.16	0.35406	2.63
9.0	0.34064	−0.69	0.35361	3.10
10.0	0.34105	−0.28	0.35394	3.49
11.0	0.34168	0.20	0.35467	4.01
12.0	0.34221	0.95	0.35525	4.79

structure appears by reconciliation of the two constraints, one from the gradient expansion, equation (29) or (34), and the other from the cusp condition which is explicitly shown by "the cusp lines" in Figure 4.

3.3 On-top density in ccPBE

In ccPBE, we have successfully applied to the proton-embedded electron-gas sphere and obtained very good results for $n(0)$ in the entire range 1−12, as given in Table 3. The TF-Kondo transition is seen by the jump in $n(0)$ at $r_s \approx 2.6$. Accuracy of the results in ccPBE is estimated by the relative error with respect to the DMC data, given in %. Note that nineteen independent data in DMC are reproduced very well by the appropriate choice of only five free parameters in ccPBE.

For the target function with $Z = 1$, which agrees with the atomic number of proton, the errors are at most about 1% but mostly much less than 1%. If we employ the target function with $Z = 2$, which is twice as large as the atomic number of proton, in determining $F_2(s)$ in equation (25) or (30), the errors are about several %, which may be said to be much larger than the case of $Z = 1$, but at the same time it may be said to be still small enough compared to the case of the original PBE. This better performance may be said to be due to the much smaller error in $\delta Z/Z$ in ccPBE, even though we do not employ the target function with the correct value of Z. Incidentally, if we calculate $n(0)$ in ccPBE with using the target function with $Z = 3$, the relative errors are found

to be still not large, ranging from –1.3% to 7.0%, about twice as large as those in the case of $Z = 2$.

4 Summary and discussion

By imposing the constraint originating from the cusp theorem on the PBE scheme in GGA to DFT, we have successfully constructed a new exchange-correlation energy functional, referred to as ccPBE (cusp-corrected PBE), and accurately reproduced the DMC data on the on-top electron density $n(0)$ in the proton-embedded electron gas with the density parameter r_s in the range 1−12.

Five comments are in order:

(i) Among fifteen parameters in the definition of $F_{\rm x}(s)$ in equation (25), only five parameters, namely, s_0, s_1, s_2, μ_1, and B_0, can be chosen freely and independently of various constraints. After a rather extensive search for appropriate values for them, we come to notice that the adequate ranges for s_1 and s_2 are limited by the cusp region $(0.32, 0.473)$ in s-variable space and probably the best values for them are those in Table 2. In this sense, $F_{\rm x}(s)$ for s in the range $s < 0.473$ is almost completely determined nonempirically by both the exact gradient expansion and the cusp theorem. As for other parameters, namely, s_0, μ_1, and B_0 having strong influence on $F_{\rm x}(s)$ for $s > 0.473$, it is still not certain whether the set of those values in Table 2 are best or not. A better set of those parameters might be found in the future.

(ii) As related to the above point, it might be considered that ρ_0 in equation (33) is another independent and important parameter, but it does not seem to be the case, because even if $\rho_0 = 1.0$ is chosen instead of $\rho_0 = 0.2$ and consequently much different values for C_i are used to define $F_2(s)$, the self-consistently determined results for $n(\boldsymbol{r})$ do not change much, indicating that we may choose any value of ρ_0 as long as it is in the physically appropriate range 0.2−1.0.

(iii) As for the choice of Z in determining the target function, it is perfectly reasonable to choose $Z = 1$ for the problems on hydrogen and the parameter set at $Z = 1$ can be applied as it is to the solid hydrogen under high pressures. Even for the case of other values of Z, we might say that ccPBE with the parameter set at $Z = 1$ may provide better results than PBE, but this needs to be confirmed by a comprehensive test of ccPBE for a wide class of real materials in the future. This test will also contribute much to the choice of best appropriate values for the parameters s_0, μ_1, and B_0.

(iv) From a fundamental point of view, the xc functional should be universal and must be determined only by the electron density $n(\boldsymbol{r})$ itself. Thus one may argue that the Z-dependent xc functional cannot be acceptable from the basic principles of DFT. In order to overcome this criticism, we may propose the following amendment: Among three terms in equation (25), only $F_2(s)$ depends on Z through the Z-dependence in $C_0, \ldots, C_6$, and s_2. Then, let us rewrite equation (30) as

$$F_2(s,Z) = \frac{p^2}{s_2(Z)^4}\left[C_0(Z) + \sum_{i=1}^{6} C_i(Z)\left(\frac{p}{s_2^2}\right)^i\right] \times \exp(-p/s_2(Z)^2). \quad (38)$$

Now, since the term $F_2(s,Z)$ becomes important only in the cusp region at which the relation of $Z = (9\pi/4)^{1/3}s/r_s$ holds, we use its relation to introduce the r_s-dependent functional $F_{\rm x}(s,r_s)$ as

$$F_{\rm x}(s,r_s) = F_0(s) + F_1(s) + F_2(s,(9\pi/4)^{1/3}s/r_s), \quad (39)$$

instead of $F_{\rm x}(s)$ in equation (25). This functional $F_{\rm x}(s,r_s)$ satisfies the basic principles of DFT and at the same time the cusp theorem will be satisfied for any Z. Note that once we consider the r_s-dependence in $F_{\rm x}$, there are additional terms in $v_\sigma^{\rm x}(\boldsymbol{r})$ in equation (15) and due changes must be made in the subsequent calculations, including the determination of the coefficients C_i and their Z-dependence. All those tasks concerning this amendment must be done before implementing a comprehensive test of ccPBE. Those works are left for the future.

(v) It is argued that the cusp theorem is satisfied in meta-GGA [35,39]. Then the DMC data in Table 1 provide a good testing ground for meta-GGA. In particular, it would be interesting to see which is the predominant scheme among several proposed ones [40–42,53–59] in reference to the DMC data.

Author contribution statement

YT as a single author has done all the works needed for the preparation of this manuscript.

References

1. Z.D. Popovic, M.J. Stott, Phys. Rev. Lett. **33**, 1164 (1974)
2. C.O. Almbladh, U. von Barth, Z.D. Popovic, M.J. Stott, Phys. Rev. B **14**, 2250 (1976)
3. E. Zaremba, L.M. Sander, H.B. Shore, J.H. Rose, J. Phys. F: Met. Phys. **7**, 1763 (1977)
4. P. Jena, K.S. Singwi, R.M. Nieminen, Phys. Rev. B **17**, 301 (1978)
5. G.W. Bryant, G.D. Mahan, Phys. Rev. B **17**, 1744 (1978)
6. G.W. Bryant, Phys. Rev. B **19**, 2864 (1979)
7. P. Jena, F.Y. Fradin, D.E. Ellis, Phys. Rev. B **20**, 3543 (1979)
8. J.K. Nørskov, Phys. Rev. B **20**, 446 (1979)
9. M.J. Stott, E. Zaremba, Phys. Rev. B **22**, 1564 (1980)
10. M.J. Puska, R.M. Nieminen, M. Manninen, Phys. Rev. B **24**, 3037 (1981)
11. M.J. Puska, R.M. Nieminen, Phys. Rev. B **27**, 6121 (1983)
12. M.J. Puska, R.M. Nieminen, Phys. Rev. B **43**, 12221 (1991)
13. J.-H. Song, Ph. D. Thesis at Oregon State University, 2004, http://hdl.handle.net/1957/29170

14. V.U. Nazarov, C.S. Kim, Y. Takada, Phys. Rev. B **72**, 233205 (2005)
15. Z.D. Popović, M.J. Stott, J.P. Carbotte, G.R. Piercy, Phys. Rev. B **13**, 590 (1976)
16. P. Jena, K.S. Singwi, Phys. Rev. B **17**, 3518 (1978)
17. A.K. Gupta, P. Jena, K.S. Singwi, Phys. Rev. B **18**, 2712 (1978)
18. P. Jena, A.K. Gupta, K.S. Singwi, Phys. Rev. B **18**, 2723 (1978)
19. J. Arponen, E. Pajanne, J. Phys. C: Solid State Phys. **12**, 3013 (1979)
20. J. Gondzik, H. Stachowiak, J. Phys. C: Solid State Phys. **18**, 5399 (1985)
21. L.M. Scarfone, A. Enver, Phys. Rev. B **43**, 2272 (1991)
22. G. Sugiyama, L. Terray, B.J. Alder, J. Stat. Phys. **52**, 1221 (1988)
23. A.I. Duff, J.F. Annett, Phys. Rev. B **76**, 115113 (2007)
24. L.H. Thomas, Proc. Cambridge Philos. Soc. **23**, 542 (1927)
25. E. Fermi, Rend. Accad. Naz. Lincei **6**, 602 (1927)
26. P. Debye, E. Hückel, Phys. Z. **24**, 185 (1923)
27. Y. Takada, R. Maezono, K. Yoshizawa, Phys. Rev. B **92**, 155140 (2015)
28. A.C. Hewson, Cambridge Studies in Magnetism, in *The Kondo Problem to Heavy Fermions*, edited by D. Edwards, D. Melville (Cambridge University Press, Cambridge, England, 1993)
29. C.A. Kukkonen, A.W. Overhauser, Phys. Rev. B **20**, 550 (1979)
30. J.P. Perdew, K. Burke, M. Ernzerhof, Phys. Rev. Lett. **77**, 3865 (1996)[1pc]
31. J.P. Perdew, K. Burke, M. Ernzerhof, Phys. Rev. Lett. **78**, 1396(E) (1997)
32. P.R. Antoniewicz, L. Kleinman, Phys. Rev. B **31**, 6779 (1985)
33. J.P. Perdew, A. Ruzsinszky, G.I. Csonka, O.A. Vydrov, G.E. Scuseria, L.A. Constantin, X. Zhou, K. Burke, Phys. Rev. Lett. **100**, 136406 (2008)
34. J.P. Perdew, A. Ruzsinszky, G.I. Csonka, O.A. Vydrov, G.E. Scuseria, L.A. Constantin, X. Zhou, K. Burke, Phys. Rev. Lett. **102**, 039902(E) (2009)
35. V.N. Staroverov, G.E. Scuseria, J. Tao, J.P. Perdew, Phys. Rev. B **69**, 075102 (2004)
36. T. Kato, Commun. Pure Appl. Math. **10**, 151 (1957)
37. A.E. Carlsson, N.W. Ashcroft, Phys. Rev. B **25**, 3474 (1982)
38. X.-Y. Pan, V. Sahnit, Phys. Rev. A **67**, 012501 (2003)
39. J.P. Perdew, A. Ruzsinszky, J. Tao, V.N. Staroverov, G.E. Scuseria, G. Csonka, J. Chem. Phys. **123**, 062201 (2005)
40. J. Tao, J.P. Perdew, V.N. Staroverov, G.E. Scuseria, Phys. Rev. Lett. **91**, 146401 (2003)
41. J.P. Perdew, A. Ruzsinszky, G.I. Csonka, L.A. Constantin, J. Sun, Phys. Rev. Lett. **103**, 026403 (2009)
42. J. Sun, A. Ruzsinszky, J.P. Perdew, Phys. Rev. Lett. **115**, 036402 (2015)
43. S. Azadi, W.M.C. Foulkes, Phys. Rev. B **88**, 014115 (2013)
44. R.C. Clay III, M. Holzmann, D.M. Ceperley, M.A. Morales, Phys. Rev. B **93**, 035121 (2016)
45. J.P. Perdew, Y. Wang, Phys. Rev. B **45**, 13244 (1992)
46. S.-K. Ma, K.A. Brueckner, Phys. Rev. **165**, 18 (1968)
47. Z. Wu, R.E. Cohen, Phys. Rev. B **73**, 235116 (2006)
48. Z. Wu, R.E. Cohen, Phys. Rev. B **78**, 197102 (2008)
49. Y. Zhao, D.G. Truhlar, Phys. Rev. B **78**, 197101 (2008)
50. C.D. Hu, D.C. Langreth, Phys. Rev. B **33**, 943 (1986)
51. P.S. Svendsen, U. von Barth, Phys. Rev. B **54**, 17402 (1996)
52. E.H. Lieb, S. Oxford, Int. J. Quantum Chem. **19**, 427 (1981)
53. Y. Zhao, D.G. Truhlar, J. Chem. Phys. **125**, 194101 (2006)
54. Y. Zhao, D.G. Truhlar, J. Phys. Chem. A **110**, 13126 (2006)
55. Y. Zhao, D.G. Truhlar, Theor. Chem. Acc. **120**, 215 (2008)
56. R. Armiento, S. Kümmel, Phys. Rev. Lett. **111**, 036402 (2013)
57. T. Aschebrock, R. Armiento, S. Kümmel, Phys. Rev. B **96**, 075140 (2017)
58. J. Tao, Y. Mo, Phys. Rev. Lett. **117**, 073001 (2016)
59. Y. Mo, R. Car, V.N. Staroverov, G.E. Scuseria, J. Tao, Phys. Rev. B **95**, 035118 (2017)